Two-electron ionization and stabilization beyond the dipole approximation

Andreas Staudt* and Christoph H. Keitel†
Max-Planck-Institut für Kernphysik, Saupfercheckweg 1, D-69117 Heidelberg, Germany
and Theoretische Quantendynamik, Physikalisches Institut, Universität Freiburg, Hermann-Herder-Straße 3, D-79104 Freiburg, Germany
(Received 21 December 2005; published 20 April 2006)

A two-dimensional model atom is employed to study the ionization behavior of helium subjected to strong laser fields in the high-frequency regime. The evolution of the system is studied by means of numerical integration of the Schrödinger equation beyond the dipole approximation. Ionization probabilities of the two-electron atom in highly intense laser fields have been calculated for different pulse shapes. It is confirmed that the mutual repulsion between the two electrons as well as the length of the laser pulses significantly alter the ionization probabilities of the system. Nondipole effects are shown to lead to a considerable increase of the ionization probabilities. For certain laser pulse shapes, a regime of ionization suppression is investigated which exists in addition to two-electron stabilization. The applicability of our model scheme to the case of heliumlike systems is discussed, and it is shown that stabilization may also occur in these systems, and how it is altered in dependence of the nuclear charge.

DOI: 10.1103/PhysRevA.73.043412 PACS number(s): 32.80.Rm, 42.50.Hz

I. INTRODUCTION

Throughout the last years, steady progress in technology has led to an overall increase in the intensity [1] and frequency [2] range of modern laser systems. Nowadays, common table-top laser systems are able to deliver pulses of such field strength to compete with or even surpass the electronic binding forces in atoms. In this intensity regime, the interaction between the light field and the atom cannot be described any more by standard perturbation theory, but the influence of both the ionic potential as well as the laser pulse on the electrons have to be treated on an equal footing. Consequently, a wealth of highly nonlinear or even relativistic effects such as above-threshold ionization (ATI) or high-order harmonic generation (HHG) start to arise [3–5].

These effects have been studied in detail and are well understood for the case of hydrogenlike atoms or ions, and naturally, the interest now focuses on complex systems such as multielectron atoms [6,7], molecules [8], clusters [9], and solids [10], where the interplay between the electrons becomes extremely important for the response of these systems to the applied laser fields.

It has been found that even for the case of helium the interaction between both electrons leads to significant modifications of the ionization dynamics, such that calculations within the single-active electron approximation are not appropriate. For instance, in the tunneling regime, the dominant mechanism for double ionization has been shown to be nonsequential, where the rescattering scenario [7,11] has been found to successfully explain the measured ionization rates: In the first step, one electron tunnels from its bound state and enters into the laser field, where it is driven away from the atom. When the relative phase of the laser changes, it is accelerated back towards its parent ion, where it may ionize the second electron by laser-assisted impact ionization. Correlated electron momentum measurements on different atomic and molecular species have corroborated the validity of this ionization mechanism [12], where deviations from this simple picture may arise from the structure of the target atoms [13] or molecules [14].

From the theoretical point of view, a variety of nonperturbative methods has been employed to address the ionization of multielectron atoms and molecules in intense laser fields, such as *S*-matrix calculations [15], density functional theory [16], classical [17] and quantum-classical approaches [18], or *R*-matrix calculations [19]. However, the most straightforward approach to this problem is the direct integration of the time-dependent Schrödinger equation. This has been carried out successfully for model systems in one [20–23], two [24–26], and three spatial dimensions [27].

To reduce the complexity of the computations, in most of the calculational methods mentioned above the dipole approximation is employed, which consists in neglecting the spatial dependence of the laser pulse, and therefore, the influence of its magnetic field on the electronic motion. However, in highly intense laser pulses, the dipole approximation is not sufficient. For a free electron subjected to the laser field, the Lorentz force leads to a displacement in the laser propagation direction. In bound systems such as atoms or molecules, this drift motion may suppress the interaction between the ionizing electron and the remaining ion. This leads to consequences for the generation of high harmonics, since here the subsequent ionization and recombination of the laser-driven electron into its ground state is essential for the emission of coherent radiation [4]. Nonsequential double and multiple ionization has also been shown to be suppressed due to this Lorentz-force induced drift [28], for in this case the electron moving in the laser field on its return to the nucleus misses the parent ion, and therefore cannot efficiently impact ionize any further electrons.

*Electronic address: staudt@mpi-hd.mpg.de
†Electronic address: keitel@mpi-hd.mpg.de; URL: http://www.mpi-hd.mpg.de/keitel/

Three-dimensional numerical calculations within the dipole approximation are despite the progress in computer technology still only feasible on high-performance facilities, whereas calculations taking nondipole terms into account are far beyond the capacity of present computer systems [29]. In contrast, in one-dimensional calculations the dipole approximation is assumed implicitly, such that the retardation of the laser pulse is neglected. Furthermore, due to the reduced phase space the interaction between both the electrons and the nucleus is overemphasized. Two-dimensional model atoms, however, are suited well to study the impact of nondipole effects on the electronic motion while the numerical complexity of the problem is seriously reduced due to the restricted phase space of the electrons.

One of the most remarkable effects arising during the interaction of atoms with strong, high-frequency laser fields is the so-called stabilization [30]. This term denotes the phenomenon that the ionization probability of an atom must not necessarily rise when the intensity of the incident laser pulse is increased, but from a certain threshold intensity this trend may be halted or even reversed. It is worthwhile to note that this is a dynamical effect arising in highly-intense, high-frequency laser fields which must not be confused with ionization suppression due to population trapping in states with small ionization cross sections [31]. Even though stabilization has been predicted by theoretical calculations in the first place, a number of experiments have confirmed the existence of this effect [32]. Experimental verification of stabilization up to now has been restricted to Rydberg atoms, since they meet the necessary condition that the photon energy must match or exceed the electronic binding energies. However, with the advent of free electron lasers [2] observation of stabilization of electrons in the atomic ground state is expected to become feasible soon. Two-electron effects in excitation and nonsequential double ionization have already been investigated for weak laser fields, and nondipole effects in general have been explored experimentally as well [5]. While two-electron stabilization has not been investigated experimentally yet, we believe this to be feasible in the future.

One instructive way to understand ground state stabilization of atoms is to switch into the eigensystem of the electron by applying the Kramers-Henneberger (KH) transformation [33,34]. In this frame, the electronic wave function is subjected to a time-varying effective potential consisting of the ionic potential superimposed by the laser field. In the limit of high laser frequencies, averaging over one period of the field for linearly polarized light results in an effective double-well potential supporting bound states. Therefore, given the wave function of the unperturbed atom may evolve into the ground state of the time-averaged KH potential, the atom may stabilize against ionization. For one-electron atoms, both analytical [35] as well as numerical calculations [36] have confirmed this view. Analytical calculations carried out in the Kramers-Henneberger frame have shown that stabilization may also occur in the case of two-electron atoms [37], such that each electron may occupy one of the potential wells. One-dimensional numerical calculations employing laser pulses of finite duration validated the existence of stabilization in two-electron systems [22], while two-dimensional calculations beyond the dipole approximation have shown that this effect is still present even when the effect of the Lorentz force on the electrons is taken into account [38].

In this paper, we present calculations giving insight into the ionization dynamics of two-electron atoms and ions in highly intense, high-frequency laser pulses. We employ a two-dimensional model system which allows us to study the time-dependent interaction between two-electron systems and electromagnetic fields beyond the dipole approximation. It is shown that stabilization indeed occurs for laser frequencies high compared to the Kepler frequencies of the electrons. The dynamic Coulomb repulsion between both electrons leads to an enhancement of the ionization probabilities of the respective two-electron systems. Stabilization, which is clearly present in the calculations performed within the dipole approximation, is diminished in the cases where the retardation of the laser pulse has been taken into account. The role of the duration of the laser pulse is examined, and it is discussed how its length and shape influences the ionization probabilities of both electrons.

II. THE MODEL ATOM

In our model, we avoid the dipole approximation by explicitly taking into account the retardation of the laser pulse. The vector potential $\mathbf{A}$ which describes the classical electromagnetic field then does not only depend on time t but also on the spatial coordinate $\mathbf{r}$, such that it reads $\mathbf{A}(\mathbf{r},t)$. We have chosen the geometry of our system in such a way that the laser pulse propagates along the y axis while the polarization direction, and therefore also the electric field, coincides with the x axis. The magnetic field then is oriented perpendicular to this plane, along the z axis. In analogy to the motion of a classical free electron in a laser field, we restrict the electronic wave functions to the plane spanned by the laser polarization and propagation direction [39,40]. The third spatial dimension is neglected in our calculations, since no notable drift into the magnetic field direction is induced due to the coupling of the electron spin to the laser field [41].

With these considerations, the vector potential can be written as $\mathbf{A}(\mathbf{r},t)=(A_x(y,t),0,0)$. It is constructed to generate oscillating electric and magnetic fields with a trapezoidal envelope function, such that the field amplitudes are linearly increased, then show a "flat-top," after which they are linearly turned off again. By choosing integer numbers of optical cycles for all the three stages of the laser pulse, no net displacement along the polarization axis as well as no momentum transfer to the electron is induced, which is a necessary condition to validate the appearance of laser-induced stabilization [42].

In our calculations, we restrict the laser parameters to the regime where nondipole and at most weakly relativistic effects may occur, while fully relativistic effects are still negligible. In its initial state, we assume the model atom to be excited, such that both electrons occupy different orbitals. This particular choice enables us to distinguish between an "inner," more strongly bound electron, and an "outer," weakly bound electron. The binding energies have been chosen to match the ionization potentials of ground state He and

He^+, respectively. It has been shown in numerical calculations [23] that differences arise in the ionization dynamics of two-electron atoms due to the symmetry of the wave function. Within this approximation we nevertheless avoid the necessity to employ an antisymmetrized electronic wave function, since in the field-free ground state the correlation between both electrons is negligible. On the other hand, when the atom is interacting with the laser pulse, the driving electric field and the Coulomb interactions between the electrons and the ion by far exceed exchange or correlation effects. In order to obtain a higher accuracy, an antisymmetrized two-electron wave function must be employed when an initial state was considered where both electrons occupy the same orbital. As mentioned above, with an electron excited this complication does not occur, and correlation and exchange effects will be neglected in what follows. It is beyond the scope of this paper to treat exchange and correlation effects in the parameter regime beyond the dipole approximation. However, we conjecture that our results hold also for this situation qualitatively, as the dynamics is dominated by the very intense laser fields considered here.

For the two-electron wave function Ψ we therefore chose a product ansatz [43]:

$$\Psi(\mathbf{r}_1,\mathbf{r}_2,t) = \phi_1(\mathbf{r}_1,t)\phi_2(\mathbf{r}_2,t). \tag{1}$$

Here, ϕ_1 and ϕ_2 denote the distinct one-electron wave functions of the inner and outer electron given at the respective positions $\mathbf{r}_1$ and $\mathbf{r}_2$ and time t.

In our model atom, both electrons dynamically interact with the laser field and each other, therefore it is an extension to the "Inner Sees Outer" [22] or "Crapola" [44] scheme. A similar model has been employed to compute the harmonic spectrum generated by the inner electron of lithium initially prepared in a Rydberg state [26].

The Hamiltonian describing the dynamics of both electrons interacting with the ionic potential V_{ion} and the laser field reads, in atomic units, with c denoting the speed of light:

$$\begin{aligned} H(\mathbf{r}_1,\mathbf{r}_2,t) = {} & \frac{1}{2}\left(\mathbf{p}_1 - \frac{1}{c}\mathbf{A}(\mathbf{r}_1,t)\right)^2 + V_{\text{ion}}(\mathbf{r}_1) \\ & + \frac{1}{2}\left(\mathbf{p}_2 - \frac{1}{c}\mathbf{A}(\mathbf{r}_2,t)\right)^2 + V_{\text{ion}}(\mathbf{r}_2) \\ & + V_{ee}^1(\mathbf{r}_1,t) + V_{ee}^2(\mathbf{r}_2,t), \end{aligned} \tag{2}$$

where $\mathbf{p}_1$ and $\mathbf{p}_2$ denote the canonical momenta of the respective electrons, while the Coulomb repulsion on each electron is mediated by the potential V_{ee}^i, $i=1,2$. In addition, to account for weakly relativistic effects, the mass shift term [45] has been incorporated in some cases into the Hamiltonian (2). It has turned out, however, that in the considered laser frequency and intensity regime this term has no notable influence on the electron dynamics, such that relativistic effects can be neglected completely in our calculations.

The interaction V_{ee}^i between both electrons is described by a mean-field ansatz, where the repulsion on each electronic wave function $\phi_i(\mathbf{r}_i,t)$ is modeled by the term

$$V_{ee}^i(\mathbf{r}_i,t) = \frac{\langle \phi_j(\mathbf{r}_j,t)|V_{ee}(\mathbf{r}_i-\mathbf{r}_j)|\phi_j(\mathbf{r}_j,t)\rangle}{\langle \phi_j(\mathbf{r}_j,t)|\phi_j(\mathbf{r}_j,t)\rangle}, \quad i \neq j; \tag{3}$$

here, the brackets indicate an integration over $\mathbf{r}_j$, while $V_{ee}(\mathbf{r})$ denotes the interaction potential between both electrons. Thus, each electronic wave function $\phi_i(\mathbf{r}_i,t)$ is subjected to the influence of the laser pulse and an effective, time-dependent Coulomb potential which consists of the sum of both the attractive nuclear potential and the repulsion due to the other electron.

In our two-dimensional model atom, the interactions between the electrons and the nucleus would be overemphasized if the bare Coulomb potential was employed. That is, the electrons would be subjected to the singularity at the origin of the ionic potential, while in a real atom they would evade the nucleus due to the higher dimensionality of the system. The effect of reduced phase space is accounted for by replacing the real three-dimensional Coulomb potentials with effective mean-field potentials, averaged over the direction perpendicular to the two-dimensional plane of motion. The interaction potentials then can be described by the so-called Rochester or softcore potential [46]:

$$V_{\text{ion}}(\mathbf{r}) = -\frac{k_{\text{ion}}}{\sqrt{\mathbf{r}^2 + a_{\text{ion}}}}, \quad V_{ee}(\mathbf{r}) = \frac{k_{ee}}{\sqrt{\mathbf{r}^2 + a_{ee}}}. \tag{4}$$

By the proper choice of parameters, one can tune the potentials (4) to reproduce the binding energies of the desired electronic configuration. For the case of helium, the parameters $k_{\text{ion}}=3.28$, $a_{\text{ion}}=1.0$ and $k_{ee}=1.15$, $a_{ee}=0.1$ lead to binding energies of 0.832 a.u. for the outer and 2 a.u. for the inner electron, corresponding to the ionization potentials of He and He^+.

III. NUMERICAL ASPECTS

A. Propagation of the wave function

To propagate the solution $\Psi(\mathbf{r}_1,\mathbf{r}_2,t)$ of the time-dependent Schrödinger equation associated with the Hamiltonian (2) with respect to time t, we employ the split-operator method [47]. By decomposing and rearranging the Hamiltonian (2), we arrive at

$$H(\mathbf{r}_1,\mathbf{r}_2,t) = H_1(\mathbf{r}_1,t) + H_2(\mathbf{r}_2,t), \tag{5}$$

where the respective one-electron Hamiltonians $H_i(\mathbf{r}_i,t)$ in the Coulomb gauge are given by

$$\begin{aligned} H_i(\mathbf{r}_i,t) = {} & \frac{\mathbf{p}_i^2}{4} + V_{\text{ion}}(\mathbf{r}_i) + \frac{1}{2c^2}\mathbf{A}^2(\mathbf{r}_i,t) + V_{ee}^i(\mathbf{r}_i,t) \\ & + \frac{1}{c}\mathbf{A}(\mathbf{r}_i,t)\cdot\mathbf{p}_i + \frac{\mathbf{p}_i^2}{4}. \end{aligned} \tag{6}$$

Both the first and the last term of Eq. (6) are diagonal in the momentum representation of the according wave function ϕ_i, while the second, third, and fourth terms are linear operators in position space. Thus, we Fourier transform the wave functions between momentum and position space, such that the application of these operators become mere multiplications.

These transformations are performed using FFT routines, which work quite fast even for numerical grids with a large number of grid points. Special care is needed for the term

$$\frac{1}{c}\mathbf{A}(\mathbf{r}_i,t)\cdot\mathbf{p}_i=\frac{1}{c}A_x(y,t)p_{i,x}, \tag{7}$$

since here operators both dependent of position and momentum couple. One way to carry out the application of this operator on the wave functions ϕ_i is to employ a combination of Fourier transformations and Crank-Nicholson schemes [39]. Yet, a more elegant way to approach this problem is to transform the x component of $\phi_i(\mathbf{r}_i,t)$ into momentum space while retaining the position space representation of its y component [48]. The operator (7) then is diagonal, such that its application on the wave function also is a multiplication. A subsequent one-dimensional Fourier transformation of ϕ_i with respect to the y component will finally result in the momentum space representation of the wave function. Employing this method to evaluate (7) has the advantage of keeping the numerical errors during the calculations consistent. No further error apart from those given by the grid partitioning and the discretization in time are introduced, which would not be the case with a mixing of different integration schemes.

One additional term which must be taken care of in the wave function propagation scheme is the repulsion between both electrons. We incorporate it in our model by taking into account the potential $V_{ee}^{i}(\mathbf{r}_i-\mathbf{r}_j)$, Eq. (3), for each electronic wave function ϕ_i. One fast and efficient way to evaluate this term is by convolving the respective electronic wave functions. At the beginning of the numerical integration, the interaction potential V_{ee} is stored on a numerical grid and transformed to momentum space. If the momentum representation of one of the electrons is multiplied by this function and transformed back to position space, we receive an effective potential representing the repulsive force acting on the other electron at this particular time step of the calculations.

The single-electron wave functions are then propagated in time by successively applying the short-time propagator

$$U_i(t,t+\Delta t)=e^{-iH_i(\mathbf{r}_i,t)\Delta t} \tag{8}$$

on each $\phi_i(\mathbf{r}_i,t)$, such that these are promoted according to

$$\phi_i(\mathbf{r}_i,t+\Delta t)=U(t,t+\Delta t)\cdot\phi_i(\mathbf{r}_i,t). \tag{9}$$

With the nearly symmetric splitting of the one-electron Hamiltonians $H_i(\mathbf{r}_i,t)$ with respect to operators which are evaluated in position and momentum space in Eq. (6), the error introduced in this propagation scheme due to the noncommutativity of the operators is of third order with respect to the discrete time step Δt [49].

To avoid reflections of the wave functions from the borders of the numerical grids which would cause unphysical interferences of the wave functions, we employ absorbing boundary conditions during our calculations. At each time step, the wave functions ϕ_i are multiplied by the radially symmetric damping function [50]

$$D(r)=\begin{cases}1 & \text{if } r\leqslant r_0,\\ e^{-4(r-r_0)^2/L_d^2} & \text{if } r>r_0.\end{cases} \tag{10}$$

The parameters r_0 and L_d must be chosen large enough that the relevant electronic dynamics which takes place in the vicinity of the nucleus is not affected by the absorbing boundary. Typical values employed during our computations were $r_0=130$ a.u. and $L_d=20$ a.u., ensuring both a large enough unperturbed interaction area of atom and laser and a smooth damping of the electronic wave packets when moving towards the edges of the numerical grid.

The range of the absolute sizes of the grids employed in our calculations has been from 150 a.u. through 200 a.u. in each spatial direction, while equidistant grid spacings between 0.15 a.u. and 0.2 a.u. have been chosen for the partitioning. By this we have ensured that the numerical grids are large enough to allow a proper evolution of the electrons in time devoid of effects introduced by the wave function damping. Also, the grid spacing is small enough to sufficiently resolve the wave packets and allow for the adequate representation of the momenta of both electrons. By adapting these crucial parameters of the numerical grids as well as the time step Δt we have ensured that convergence of the results has been achieved in our calculations.

B. Determination of the ionization probability

One important quantity we want to determine in our computations is the ionization probability of the electrons. Calculating it by projecting the wave functions onto the field-free bound states of the atom is not appropriate for our system, since the computation of all two-electron states necessary to gain good enough convergence of this method would be far too complex to handle. On the other hand, due to the finite grid size and therefore the limited momentum spectrum, projecting onto the field-free continuum states of the ionic potential would surely also not reproduce the correct ionization probabilities of the system.

One established method of calculating the ionization probabilities in numerical calculations is to determine the amount of the electronic wave packets remaining in a defined region around the nucleus after the interaction with the laser pulse [22,27,38,51]. However, this method has the drawback that the number of continuum states is artificially enlarged, with the result that depending on the size of this region some highly excited bound states are also considered being ionized.

In our calculations, we employ an alternative approach to define the ionization probability P_i for each electron by considering those parts of the wave function ϕ_i being ionized that have positive total energy. In close analogy to classical mechanics we expect all portions of the wave functions whose kinetic energy exceeds their negative potential energy to leave the parent ion and become ionized. By defining P_i through

$$P_i=1-\int_{-\infty}^{0}|\hat{\phi}_i(E)|^2dE, \tag{11}$$

where $\hat{\phi}_i(E)$ denotes the representation of the wave function in energy domain, we additionally account for those parts of

ϕ_i which have been damped by the absorbing boundary of the numerical grid during the interaction with the laser pulse. The local potential and kinetic energy densities are calculated in position space. The potential energy then can be determined exactly at every grid point, while the kinetic energy is calculated using a two-dimensional five-point formula for the second derivative [52]. The latter has been found to be sufficiently accurate for the grid partitioning employed in our calculations.

Our method of determining the ionization probability has been tested for different configurations of the numerical grid, and is virtually independent of both the total grid size as well as of the distance between the consecutive grid points. The consistency of this approach has been furthermore validated by performing calculations where the wave functions have been propagated for an additional number of optical cycles after the laser pulse has been ramped down. During this time, most of the ionizing fractions of the wave packets move towards the edges of the numerical grid where they are damped by the absorbing boundary. The resulting ionization probabilities calculated via Eq. (11) have been found to coincide with those which have been calculated directly after the laser pulse has been turned off. Furthermore, for single-active electron calculations we have verified this method by projecting out up to eight bound states of the wave function before determining the ionization probabilities, which quantitatively yielded the same results.

Although the definition of the ionization probability via Eq. (11) may not be strict in a quantum-mechanical sense, it is nevertheless more appropriate than defining an arbitrary border separating bound and ionized electronic states. Notice, however, that in general both methods qualitatively yield similar results.

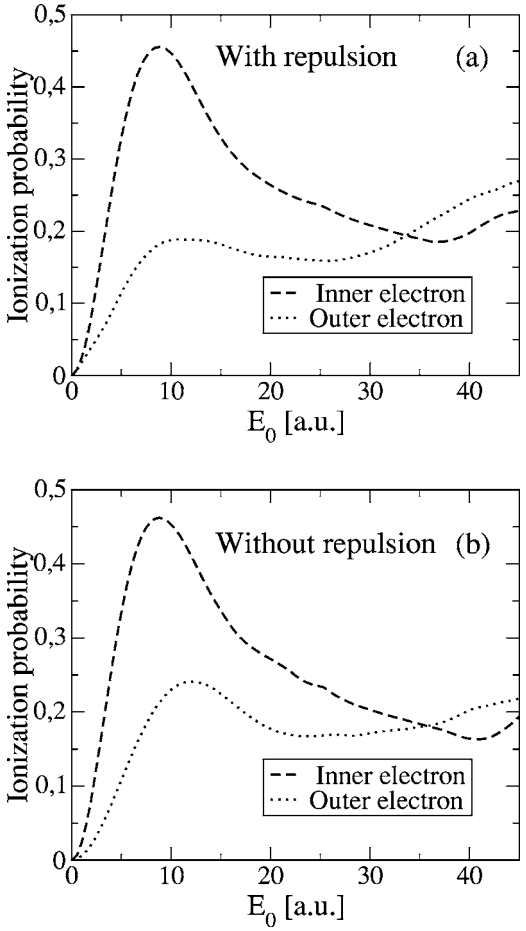

FIG. 1. Ionization probabilities of the inner and the outer electron as a function of the peak electric field strength E_0. The frequency of the laser is ω=3 a.u., while the pulse consists of each four optical cycles linear turn-on and turn-off, and eight optical cycles at fixed amplitude. In (a), the ionization probabilities are displayed for the case where the repulsion between the two electrons has been taken into account, while it has been neglected in (b).

IV. RESULTS AND DISCUSSION

In this section, we discuss the ionization dynamics of the model atom subjected to highly intense, high-frequency laser pulses. The laser parameters are chosen such that stabilization of the two-electron system may occur. First, results for helium are presented, and the influence of the repulsion between both electrons on the ionization probabilities is analyzed. In Sec. IV B, we investigate the role of the retardation of the laser pulse on the wave packet dynamics and the ionization probabilities in the stabilization regime. In the subsequent section, the influence of the laser pulse shape on the atomic dynamics is discussed. Finally, in Sec. IV D we extend our model system to the case of lowly charged two-electron ions, where we study their interaction with laser pulses of such intensity and frequency that these systems may stabilize against ionization as well.

A. Ionization of helium at high frequencies

In this section we present the ionization probabilities of helium in the high-frequency regime, at a laser frequency where stabilization of the atom is likely to occur. A general yet quite conservative condition for the appearance of stabilization is that the energy of a single laser photon field must exceed the ionization potential of the bound electron. For helium in the ionic or atomic ground state, this implies laser frequencies ω higher than 2 a.u. or 2.9 a.u., respectively.

Displayed in Fig. 1 are the ionization probabilities of the inner and the outer electron subjected to a laser pulse of angular frequency ω=3 a.u., which clearly fulfills the condition mentioned above. The pulse shape consists of four optical cycles linear ramping-up, followed by eight cycles at constant peak electric field strength E_0 and four cycles linear turn-off. The choice of four cycles for the turn-on of the laser pulse is short enough to inhibit significant ionization before the atom is exposed to the maximum intensity of the laser pulse [53]. Its duration is nevertheless long enough to suppress shake-up and shake-off processes which would occur if the increase in field strength was too rapid. Speaking in terms of the quasistationary Kramers-Henneberger frame, a sudden turn-on of the laser leads to a population transfer to excited states of the KH potential due to the finite bandwidth of the pulse, while in the case of a smooth turn-on the electronic wave function may evolve into its ground and low-

lying states and therefore become stabilized against ionization.

As can be seen from Fig. 1(a), both the electrons at this high frequency indeed exhibit the stabilization effect. After a steady increase in ionization probability with laser intensity, beyond a certain threshold intensity the atom becomes stable in the laser field, where both electrons show different ionization signals. Due to its stronger interaction with the nucleus, for smaller field strengths the inner electron shows a higher probability to be found ionized after the interaction with the laser pulse than the outer. At a field strength $E_0=8.8$ a.u., at the onset of stabilization, the ionization probability P_1 of the inner electron is 2.5 times as large as that of the outer. When the field strengths are further increased, the atomic ionization behavior starts to become highly nonperturbative, and stabilization sets in, which is most prominent for a field strength of about $E_0=37$ a.u. At even higher intensities, the stabilization effect breaks down, and the ionization probability again increases with the laser field strength. For the outer electron, we also observe in the region from $E_0=11$ a.u. to $E_0=27.5$ a.u. that the ionization probability P_2 ceases to increase with laser intensity, yet the stabilization effect is not clearly pronounced. As in the case of the inner electron, P_2 rises again steadily at higher laser intensities ($E_0>30$ a.u.).

To study the influence of the repulsion between both electrons on the stabilization of the helium model atom, calculations have been carried out where the interaction between both the electrons has been discarded. The calculations then effectively become single-active-electron computations, where the ionization potentials are chosen to match those of the inner and the outer electron of the product wave function Eq. (1). The results of these calculations are displayed in Fig. 1(b). For the inner electron, the ionization probabilities virtually coincide with those of the interacting case for small peak electric field strengths. Increasing these to values higher than $E_0=25$ a.u., both notably start to differ, where the ionization probabilities in the interaction case exceed those calculated without repulsion. For the latter, the breakdown of the stabilization effect sets in at a higher peak field strength $E_0=41$ a.u., while at the highest field strength depicted in Fig. 1, $E_0=45$ a.u., the ionization probability P_1 is 15% smaller than in the calculations where the repulsion has been taken into account. The role of the electronic repulsion on the ionization of the two-electron atom is more pronounced for the outer electron. Here, in contrast to Fig. 1(a), a distinct maximum in ionization is visible at a field strength $E_0=12$ a.u. before the stabilization effect sets in. The stabilization begins to break down at $E_0=28$ a.u., where the increase in P_2 sets in rather smoothly. For the largest field strength calculated, the ionization probability is by 20% smaller than in the interacting case. Thus, we find that even though the electronic repulsion does not inhibit the stabilization of the helium atom, it leads to modifications in contrast to single-active electron calculations. Most notably, in the region of high intensities an increase in the ionization probabilities can be observed.

B. Influence of nondipole effects

As discussed earlier, the retardation of the laser field leads to a displacement of the electrons in the laser propagation direction, modifying the overall ionization dynamics of the two-electron atom. As a consequence, the stabilization effect may be suppressed at higher laser intensities [40,54], since with the inclusion of the laser retardation the periodicity of the Kramers-Henneberger potential with respect to time is abolished. Signatures of nondipole effects can be clearly observed from the structures of both electronic wave functions $\phi_i(\mathbf{r}_i,t)$ during the interaction with the laser field. In Figs. 2(a) and 2(b), the probability densities of the respective wave functions of the inner and outer electron are displayed, after the helium atom has been exposed to a laser pulse consisting of four optical cycles turn-on and six cycles at peak electric field strength $E_0=45$ a.u. and frequency $\omega=3$ a.u.

One can observe an asymmetric distribution of the wave functions with respect to the laser polarization direction. Notable amounts of the wave packets are transferred into the laser propagation direction, along the positive y axis, which is due to the retardation of the laser pulse. The laser electric field depends on the position in the propagation direction, therefore parts of the electronic wave packets at different positions are subjected to different electric field strengths. This leads to a net force driving the electronic wave packets in the laser propagation direction. In a classical sense, this drift motion can be understood to be caused by the momentum transfer of the photon field to the electron [39]. This finding is in clear contrast to the results which are obtained when employing the dipole approximation. As can be seen from Figs. 2(c) and 2(d), when the dipole approximation is carried out the respective wave functions of both electrons are distributed symmetrically along the laser polarization axis. One further, interesting feature is the localization of significant parts of the wave function near the nucleus along the polarization axis, which is best visible for the inner electron, Figs. 2(a) and 2(c). These structures arise due to the dichotomous structure of the effective potential the electrons sense during their interaction with the high-frequency laser pulse at constant field strength. The wave functions tend to redistribute to occupy the ground state of the according KH potential, which exhibits two maxima separated from each other by twice the quiver amplitude $\alpha_0=E_0/\omega^2$. This dichotomy, however, does not clearly show up in the electron densities displayed in Fig. 2, since at the moderate value $\alpha_0=5$ a.u. at these laser parameters the maxima of the soft-core potential in the time-averaged KH frame are not well separated. The wave functions are therefore merely smeared out along the x axis. Only for larger values of α_0, as has been shown in Ref. [38], the wave function densities exhibit distinct maxima at the extremal points $x=\pm\alpha_0$. This effect, however, is diminished by the rising and falling edges of the laser pulse and its finite duration, resulting in the appearance of additional structures between these two points [55].

To get an intuitive understanding of the underlying atomic dynamics, one may identify the electronic wave packets with classical pointlike charged particles. In this sense, we associate the wave packets by their respective position expectation values

$$\langle \mathbf{r}(t)\rangle_i = \int \mathbf{r}\,|\phi_i(\mathbf{r},t)|^2 d\mathbf{r}. \tag{12}$$

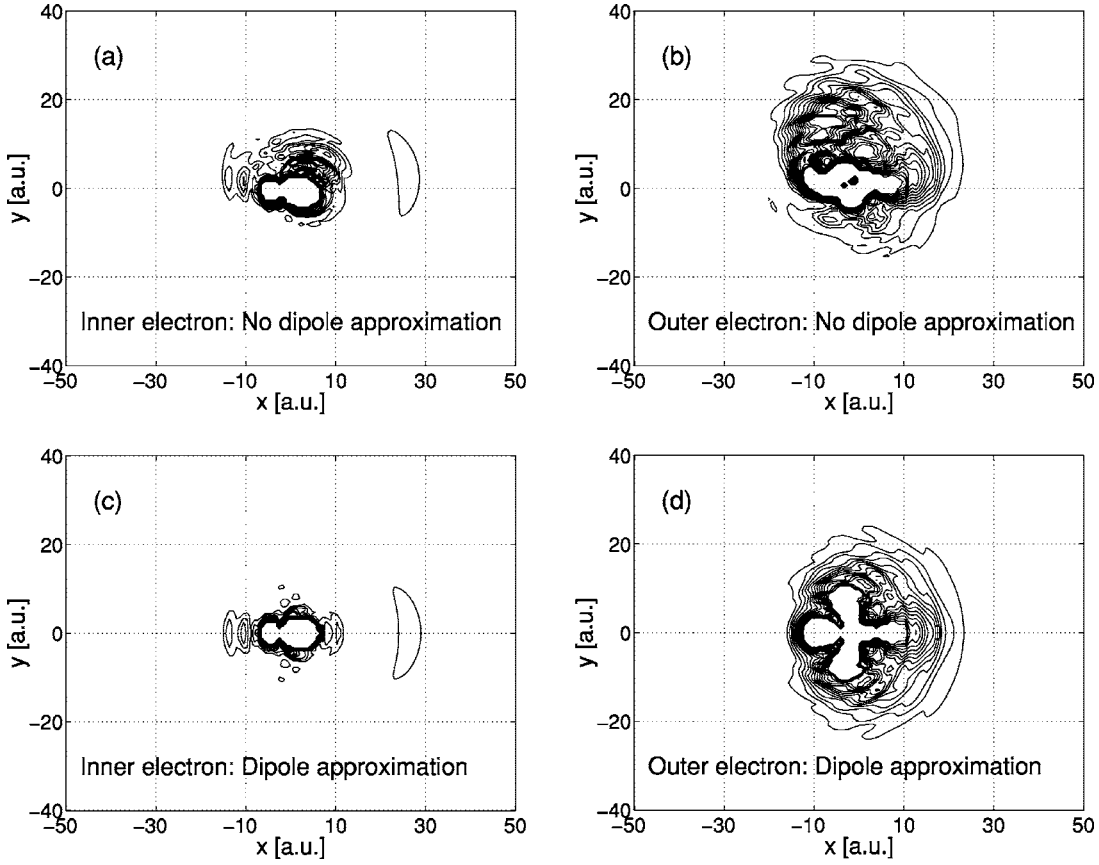

FIG. 2. Contour plots of the inner (a) and outer (b) electron probability density after 10 cycles interaction with the same laser pulse as in Fig. 1, at peak field strength $E_0=45$ a.u. The x axis is the polarization direction of the laser field, while the laser propagates along the y axis. Here, the dipole approximation has not been carried out in the computations, such that the retardation of the laser pulse has been taken into account. In the lower row, subfigures (c) and (d), the electron densities are displayed for calculations which have been performed within the dipole approximation. For better visibility, 15 contour lines are shown for a density range between 0 and 1×10^{-3}.

Displayed in Fig. 3 are the center-of-mass positions of both electrons as a function of time, while interacting with a laser pulse of peak electric field strength $E_0=45$ a.u. and frequency $\omega=3$ a.u. In Fig. 3(a), the motion of both electrons in the polarization direction is depicted. One can clearly observe the close analogy to the motion of a classical particle. After the turn-on stage, both electrons oscillate with an excursion amplitude equal to the quiver radius $\alpha_0=5$ a.u. An additional effect occurring here is the overall motion of the inner electron's mass center in the positive polarization direction, while the wiggling of the outer electron is almost symmetric with respect to the laser polarization axis. This displacement is caused by the combined effect of the nucleus and the laser field on the evolution of the wave packets during the turn-on of the pulse [25]. At a certain phase of the laser pulse, the strength of the electric field surpasses the force of the nucleus acting on the electrons, such that they are ejected with a net drift along the polarization axis. Due to the difference in binding energies, this phase, and therefore also the drift motion of both electrons differ. This overall motion along the polarization axis is in contrast to that of a free electron in the laser field, which is symmetric with respect to its initial point at rest. Notice that this effect becomes important especially in the intensity domain in which the stabilization effect breaks down, where it suppresses the population of bound states of the static Kramers-Henneberger potential in combination with nondipole effects. The influence of the retardation of the laser pulse becomes apparent when the drift of the electrons in the laser propagation direction is considered, which is visualized in Fig. 3(b). For comparison, the projection of the motion of a free electron subjected to the same laser pulse onto the laser propagation axis is also displayed as a function of time. As already concluded from Figs. 2(a) and 2(b), notable amounts of the wave packets are transferred in the laser propagation direction. The total displacement of the outer electron is 6 a.u. in the laser propagation direction, which even exceeds the maximum excursion amplitude $\alpha_0=5$ a.u. in the laser polarization direction. The extent of the excursion in the laser propagation direction of the outer electron becomes comparable to that of the free electron of 9.2 a.u., which can be attributed to the weaker attraction of the nucleus. The role of the latter becomes best visible during the turn-off phase of the laser pulse, in the range between 12 and 16 optical cycles, where the mass center $\langle \mathbf{r}(t)\rangle_2$ of the outer electron is clearly accelerated back towards the parent ion. The inner electron is due to its tighter binding to the nucleus not as much affected by the retardation of the laser pulse as the outer electron, yet in analogy to Fig. 2(a) a transfer of the mean of the wave packet in the laser propagation direction

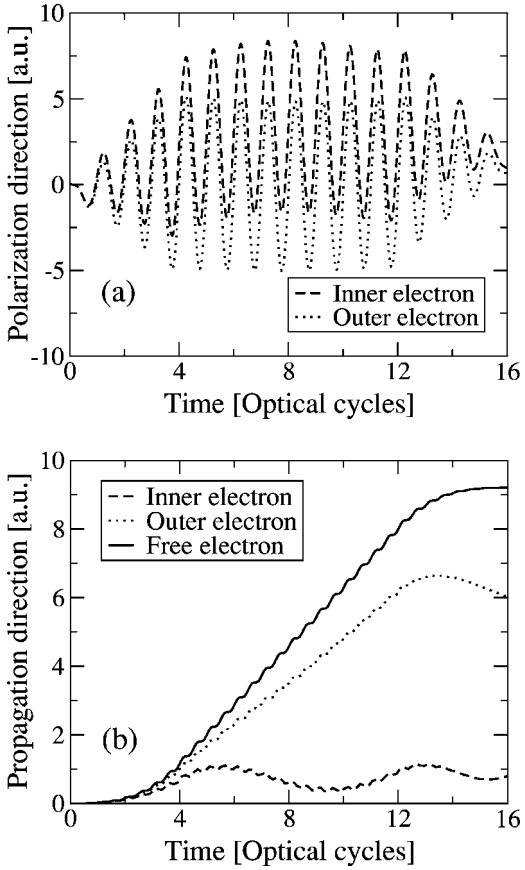

FIG. 3. Displacement of the center of masses of the electrons along the laser polarization axis (a), and in the propagation direction (b) as a function of time. As in Fig. 1, the pulse consists of each four optical cycles linear turn-on and turn-off, and eight cycles at maximal field strength $E_0=45$ a.u. and frequency $\omega=3$ a.u. For comparison, the displacement of a classical electron subjected to the same laser pulse in the propagation direction is also shown in (b).

can be observed. However, its value of 0.8 a.u. at the end of the laser pulse is small compared to both that of the outer electron and the quiver amplitude, such that no notable nondipole effects are expected to arise in the ionization probabilities of the inner electron.

To quantify these effects showing up in the overall wave packet dynamics, we have carried out calculations in which the dipole approximation has been assumed by explicitly removing the spatial dependence of the vector potential $\mathbf{A}(\mathbf{r},t)$. As expected, in the case of the inner electron the influence of the retardation of the laser pulse on the ionization probability is almost negligible, with the results gained from the nondipole computations exceeding those calculated within the dipole approximation only slightly in the intensity regime where the stabilization effect breaks down. The situation becomes quite different for the outer electron, which can be seen in Fig. 4, where we compare the ionization probabilities taken from Fig. 1 with calculations, where the dipole approximation has been carried out.

For peak field strengths up to $E_0=20$ a.u., both sets of calculations virtually yield the same result. At this field strength, the velocity of the electron is roughly 5% of the speed of light, and as expected in this regime, weakly relativistic effects start to occur. The Lorentz force then promotes the ionization, such that for higher field strengths the results start to differ. For the largest field strength $E_0=45$ a.u. calculated, the nondipole result shows an ionization probability which is about 14% higher than that which has been obtained within the dipole approximation.

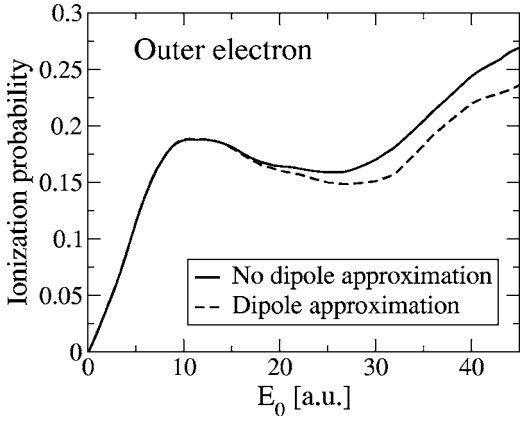

FIG. 4. Ionization probabilities of the outer electron as a function of the peak electric field strength E_0, where either the retardation of the laser pulse has been taken into account or has been neglected (dipole approximation). The laser pulses have been chosen to be the same as in Fig. 1, while for better visibility the scale has been changed.

C. Pulse-length dependence of ionization

In this section, we investigate the role of the length of the laser pulse on the ionization of the helium model atom in the high-frequency regime. We do this by altering the shape of the laser pulse by varying the length of the turn-on and turn-off and the intermediate stages of the field. For convenience, we choose a pulse profile where the number of turn-on cycles equals those of the turn-off, such that the pulse envelope becomes symmetric with respect to time. By altering the number of turn-on and turn-off cycles of the trapezoidal pulse, we are able to identify effects caused by the electron dynamics during the stages of change in peak intensity, while by changing the number of cycles in the center part of the pulse one may observe ionization of the electronic population which has already been trapped in the quasistationary Kramers-Henneberger potential.

In the first step, we reduce the adiabacity of the laser pulse by decreasing the number of turn-on and turn-off cycles of the pulse. In Fig. 5, the ionization probabilities of the inner and outer electron are displayed, where the electronic repulsion has either been taken into account in the calculations (a) or neglected (b). Notice that this is a similar pulse as that employed in the previous calculations, but with the length of turn-on and turn-off stages reduced to two optical cycles each. Even though the overall ionization probabilities of both electrons resemble those displayed in Fig. 1, a lot of subtle differences can be observed. While in the calculations employing shorter pulses, Fig. 5(a), the stabilization effect of the inner electron and its subsequent breakdown at higher field strengths is more distinct when sub-

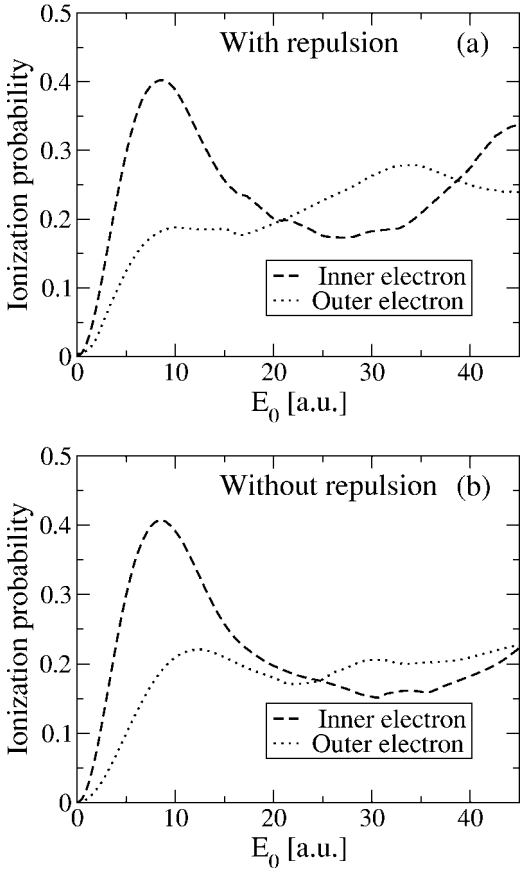

FIG. 5. Ionization probabilities of the inner and the outer electron as a function of the peak electric field strength E_0. The frequency of the laser is $\omega=3$ a.u., while the pulse consists of each two optical cycles linear turn-on and turn-off, and eight optical cycles at fixed amplitude. In (a), the ionization probabilities are displayed for the case where the repulsion between the two electrons has been taken into account, while it has been neglected in (b).

jected to the laser pulse of shorter duration, stabilization of the outer electron merely vanishes. For the latter, ionization rather saturates for field strengths ranging between $E_0=9.5$ a.u. and $E_0=17$ a.u., before a further increase sets in. The stabilization effect of the outer electron is more pronounced when the repulsion between both electrons is neglected, Fig. 5(b). Here, a steady decrease of the ionization probability in the range from $E_0=12$ a.u. to $E_0=23$ a.u. is clearly visible. Apart from this feature, the overall ionization probabilities of the inner and outer electron for field strengths up to $E_0=20$ a.u. are quite insensitive to their mutual interaction, while at higher intensities the Coulomb repulsion between both electrons promotes the ionization.

A remarkable effect sets in for field strengths exceeding $E_0=34$ a.u. The curve of the outer electron exhibits a notable drop, while the inner electron's ionization probabilities at these intensities are slightly increased, compared to the results shown in Fig. 1. Additional calculations at peak field strengths E_0 exceeding those for which results have been shown in Fig. 1 reveal that this ionization suppression of the outer electron vanishes at higher intensities. This effect, albeit not as prominent as in Fig. 5(a), also occurs for the outer electron when the electronic repulsion has been discarded, at peak field strengths about $E_0=32$ a.u., Fig. 5(b).

The additional ionization suppression becomes even more prominent when the duration of the turn-on and turn-off stages are further reduced, i.e., when pulses of 10 optical cycles total duration with each one cycle turn-on and turn-off are employed. On the other hand, by increasing the length of the laser pulse turn-on and turn-off stages to three cycles this change in the slope of the curves for both electrons merely vanishes.

To gain further insight into the pulse-shape dependence of the ionization probabilities, we have in a second step performed calculations in which the length of the center part of the pulse envelope, and therefore the number of laser cycles at constant peak intensity has been varied. While keeping the turn-on and turn-off stages of the pulse fixed at four optical cycles each, center parts with lengths ranging from four to 12 cycles have been employed. In contrast to variations of the turn-on and turn-off stages, we observe mostly quantitative changes in the ionization probabilities of the inner electron, Fig. 6(a). The most prominent changes occur in the maxima of the curves at low intensities, which mark the onset of nonperturbative atomic dynamics. The ionization probability P_1 at this point increases linearly with the number of optical cycles at peak intensity. Concomitantly, the peak field strength E_0 at which stabilization sets in is progressively slightly shifted to smaller values. This is a similar behavior to that found in the stabilization of hydrogen in ultrashort laser pulses [56]. However, the ionization probability at the point of maximum stabilization is barely affected by the change of pulse length, leading to the overall result that the stabilization effect of the inner electron becomes more prominent when the number of optical cycles at constant peak intensity is increased.

For the outer electron, Fig. 6(b), the evolution of the ionization curves with increasing pulse length is more complex. The maxima in the curves P_2 at the onset of stabilization are centered at field strength $E_0=10.5$ a.u., with the ionization probabilities progressively increasing with the total duration of the pulse. The maximum and the point of optimal stabilization of the outer electron become more and more pronounced, the longer the laser pulse. When the number of optical cycles at constant peak field strength exceeds nine, the ionization suppression effect already noted in Fig. 5 sets in, while its position is shifted to lower peak intensities. Test calculations employing pulse lengths with intermediate stages of 20 cycles duration confirm the persistence of this ionization suppression regime of the outer electron for even longer pulse durations.

We have found that the existence of this effect is due to the specific preparation of the initial state of the model atom, where the outer electron is placed in the excited $2s$ state. When subjected to laser pulses of long durations compared to the length of the turn-on and turn-off stages, population may be dynamically transferred from the excited state to the ground state of the atom, which leads to a notable ionization suppression. A thorough discussion of this effect for one-electron atoms is given elsewhere [57].

D. Ionization of heliumlike ions

We now discuss the general applicability of our model atom scheme to the case of two-electron ions. This is of

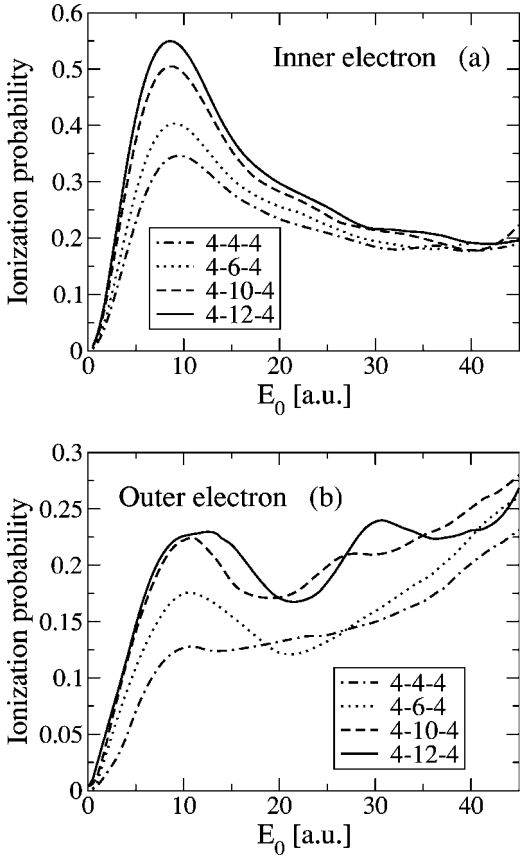

FIG. 6. Ionization probabilities of the inner and the outer electron of helium for varying pulse lengths. The frequency of the laser is $\omega=3$ a.u., with the pulse consisting of each four optical cycles linear turn-on and turn-off, and a center part of constant amplitude E_0 with a length of 4, 6, 10, and 12 cycles, respectively. In (a), the ionization probabilities are displayed for the inner electron, while in (b) those of the outer electron are shown. The numbers in the caption refer to the length (in optical cycles) of the turn-off, intermediate, and turn-off stages of the laser pulses employed throughout the respective calculations.

particular interest, for in contrast to the ionization and especially stabilization behavior of hydrogenlike ions [58] the relevant parameters governing the atomic dynamics do not trivially scale with the charge state Z [59]. This is due to the variations of interaction strength between both active electrons for different two-electron systems. Consequently, we expect the ionization rates for two-electron ions to differ qualitatively as well as quantitatively from those of helium.

Since a nonrelativistic description of the atomic or ionic dynamics is employed, the model scheme is restricted to the case of He-like ions of low charge state Z. Otherwise, the high space charge in the vicinity of the nucleus would force us to incorporate higher-order correction terms such as the electron spin or the relativistic mass-shift into the Hamiltonian (2) to take account of first-order relativistic effects [45].

A second restriction in the applicability of our model scheme to two-electron ions arises from the choice of softcore parameters for reproducing the correct ionization potentials of the electrons. With increasing Z, the binding energies of the inner and outer electron tend to differ more from each other, an effect which can only be compensated for by increasing the parameters a_{ion} and a_{ee} in Eq. (4). However, the larger these parameters, the more the softcore potentials deviate from the real Coulomb potential, such that the approximation of reduced dimensionality becomes questionable. One way to circumvent this problem would be to place the outer electron initially into a highly excited state, which may cause undesired physical features due to the intermediate atomic levels.

Therefore, in the following we will consider the two ions with lowest charge Z, which are Li^+ and Be^{2+}. As in the case of the helium atom, we employ an excited initial state with both electrons occupying different orbitals, while their respective binding energies are chosen to match the ionization potentials of the corresponding two-electron ions with electrons in the same $(1s)$ state. The choice of the softcore parameters $k_{\mathrm{ion}}=8.676$, $a_{\mathrm{ion}}=2.2$ and $k_{ee}=1.855$, $a_{ee}=0.17$ in Eq. (4) reproduces the ionization energies for Li^+, which are 4.5 a.u. for the inner and 2.7 a.u. for the outer electron. For Be^{2+}, we have found the parameters $k_{\mathrm{ion}}=15.23$, $a_{\mathrm{ion}}=2.45$ and $k_{ee}=2.48$, $a_{ee}=0.193$ to generate the binding energies of 8 a.u. and 5.4 a.u. for the inner and outer electron, respectively.

As has been shown in Sec. IV C, interesting features show up in the ionization yields when laser pulses with short rising and falling edges are employed [60]. Therefore, as in Fig. 5 we will consider pulses with each two optical cycles turn-on and turn-off and eight cycles at constant intensity. In Fig. 7(a), the ionization probabilities of both electrons are shown for the lithium ion, where the laser frequency $\omega=5$ a.u. has been employed in the calculations. At this frequency, the energy of a single photon surpasses the ionization potential of each of the electrons, yet the absorption of at least two photons is necessary to allow for double ionization. Similar to the case of helium, Fig. 5, we also find stabilization to occur in this system. Due to the higher laser frequency and stronger binding of the electrons, higher field strengths are necessary to transfer the ion into a physical regime where nonperturbative ionization behavior occurs. In contrast to helium, the ionization probabilities behave similar up to a field strength $E_0=50$ a.u., where the stabilization effect of the outer electron breaks down, while for the inner electron the breakdown of stabilization sets in at a higher field strength $E_0=70$ a.u.

The role of the repulsion between the two electrons is revealed by comparing the ionization probabilities to those that have obtained from calculations where the interaction potential V_{ee} has been neglected, displayed in Fig. 7(b). Here, the overall ionization probabilities of both electrons are smaller than in the interacting case, especially those of the outer electron. At the highest peak field strength $E_0=100$ a.u. employed in our calculations, for both electrons the ionization probability in the interacting case is about 60% higher than in the noninteracting case. When the repulsion is taken into account, the maxima in the ionization curves are shifted to lower intensities, which is a clear indication for the energy transfer between both electrons. While the onset of nonperturbative behavior for the outer electron is at a higher field strength than that of the inner, the stabilization effect

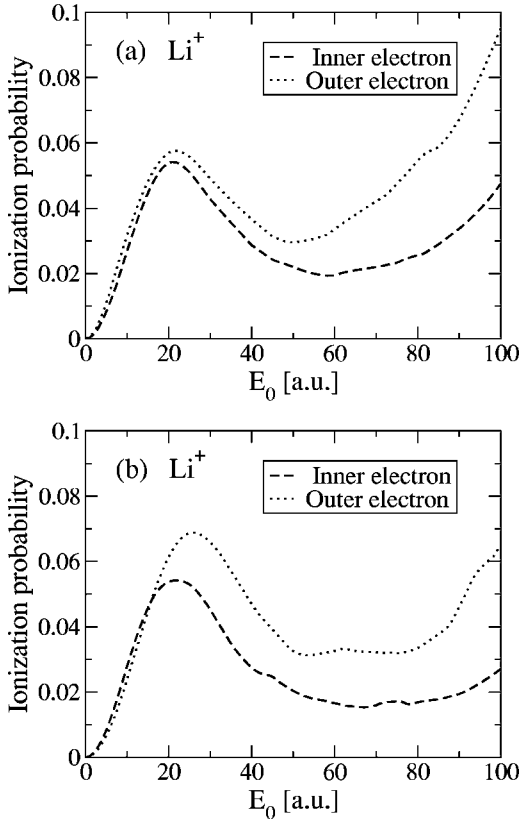

FIG. 7. Ionization probabilities of the inner and the outer electron of Li^+ as a function of the peak electric field strength E_0. The frequency of the laser is $\omega=5$ a.u., while the pulse consists of each two optical cycles linear turn-on and turn-off, and eight optical cycles at constant amplitude. In (a), the ionization probabilities are depicted with the repulsion between both electrons being taken into account, while it has been neglected in (b).

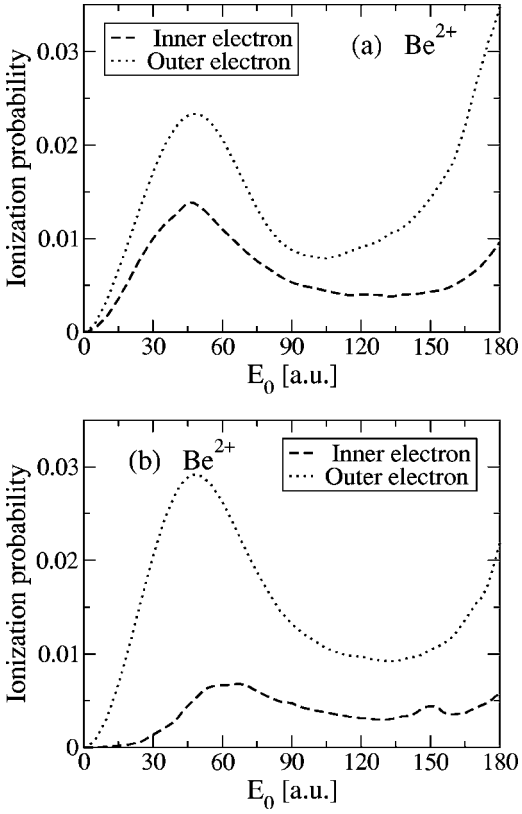

FIG. 8. Ionization probabilities of the inner and the outer electron of the doubly charged beryllium ion. The frequency of the pulse is $\omega=7.5$ a.u., while its shape consists of each two optical cycles linear turn-on and turn-off, and eight optical cycles at constant peak electric field strength E_0. Depicted in (a) are the ionization probabilities when the repulsion between both electrons is taken into account, while it has been neglected in (b).

breaks down at smaller peak field strengths, that is, at $E_0=80$ a.u. as opposed to $E_0=85$ a.u. As in helium, the energy-sharing between both electrons in Li^+ thus enhances ionization and also promotes the breakdown of stabilization in the high-intensity regime. By comparing the results displayed in Figs. 1 and 5, we find that the electron repulsion has a higher impact on the ionization probabilities than in the case of the helium atom. For the latter, the maximal increase in the ionization probabilities of each electron is about 20%, compared to about 60% for each electron in the case of Li^+ for the highest peak field strengths considered here. Our calculations have also shown that for the lithium ion in the high-frequency regime laser retardation effects play an important role, leading to an overall increase of the ionization probabilities of about a half compared to the results calculated within the dipole approximation. In addition, we observe a small feature at $E_0=74$ a.u. in the ionization probabilities of the inner electron. This can be attributed to a resonant transition caused by the small duration of the turn-on and turn-off stages of the laser pulse, which is confirmed by the absence of this structure when the pulse is ramped up and down more slowly.

We now focus our interest on doubly charged beryllium, the other two-electron ion we have carried out calculations for employing our model atom. In Fig. 8 we display the probabilities of the inner and outer electron of Be^{2+} to be found ionized after the ion has been exposed to the laser pulse of frequency $\omega=7.5$ a.u. Notice that while laser pulses of the same shape as in the calculations for Li^+ have been employed, the situation is different, since now the energy of one photon is smaller than the binding energy of the inner electron. At least two photons must be absorbed to energetically allow for double ionization. As in the case of Li^+ stabilization occurs in this system as well. Both electrons show a maximum in ionization at a field strength $E_0=48$ a.u., followed by a steady decrease. Only for field strengths exceeding $E_0\approx 130$ a.u., a breakdown of the stabilization effect sets in. The importance of mutual energy sharing between both electrons is stressed by analyzing the ionization probabilities in the case when the repulsion is neglected, as depicted in Fig. 8(b). Here, the ionization behavior of both electrons drastically changes. In the noninteracting case, the ionization probabilities P_2 of the outer electron are higher than in the case where the electronic repulsion has been taken into account, while they are smaller for the inner electron. The maximum of ionization of the latter also is shifted to a higher field strength $E_0=64$ a.u. This discrepancy between the ionization probabilities in Figs. 8(a) and 8(b) is a strong indication for the importance of the electronic interaction for the

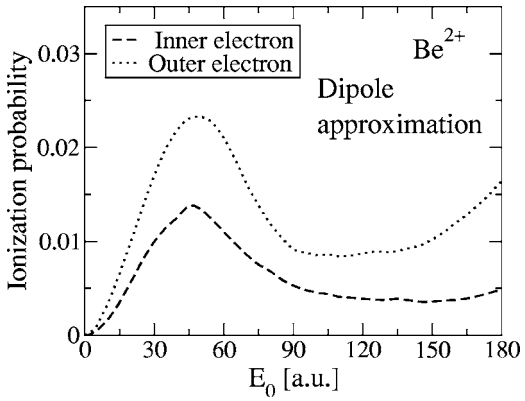

FIG. 9. Same as Fig. 8(a), but here the dipole approximation has been employed throughout the calculations.

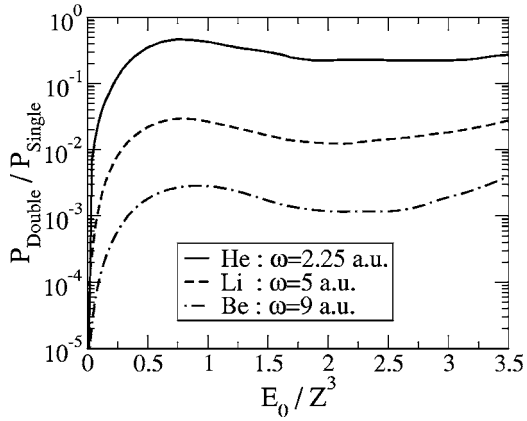

FIG. 10. Ratio of double to single ionization probabilities for the three two-electron systems after interaction with a laser pulse of 12 cycles total duration, where in each case the frequency ω has been chosen to slightly exceed the binding energy of the respective inner electron. To allow for comparison of the curves, the peak field strength E_0 has been scaled with $1/Z^3$.

ionization and stabilization process. For both electrons, for the highest field strengths displayed in Fig. 8 the ionization probabilities are increased at about 65% as compared to the calculations where the electronic interaction term V_{ee} has been neglected. Overall, the increase in ionization due to the electronic interaction is more distinct than for the lithium ion, showing that in the stabilization regime the mutual energy sharing between both electrons becomes more important with increasing nuclear charge Z.

To emphasize the importance of the retardation of the laser pulse we present in Fig. 9 results for the ionization of Be^{2+} at a frequency $\omega=7.5$ a.u. within the dipole approximation. The nondipole effects in the beryllium ion at these parameters are even more prominent than in helium (see Fig. 4) and Li^+. Comparing to the curves in Fig. 8(a), where the retardation of the laser pulse has been taken into account, one clearly observes the breakdown of the dipole approximation in the intensity regime where the stabilization effect breaks down. The Lorentz force induced drift of the electronic wave packets visibly promotes the ionization of the two-electron system. For the largest peak field strengths considered in our calculations, at $E_0=180$ a.u., the ionization probabilities are nearly twice as high when the retardation of the laser pulse is taken account of compared to the calculations within the dipole approximation.

Principal differences in the ionization dynamics of the three two-electron systems considered here arise from the different nuclear charges and electronic interaction strengths. With increasing charge Z the absolute differences in the binding energies between inner and outer electron tend to increase; therefore, the outer electron is expected to ionize more rapidly which effectively leads to a decrease in the electronic interaction. In addition, to overcome the increasing binding energies also higher peak field strengths must be employed to allow for the observation of stabilization and its breakdown, such that the forces due to the driving laser field acting on the electrons becomes stronger in the ionic case than with helium.

However, the main influence on the differences in the ionization dynamics result from the tighter binding of the electrons in the initial state, which becomes more important with increasing ionic charge. This is due to the fact that with larger Z the electronic wave functions tend to be more closely confined to the nucleus, resulting in a stronger interaction between both electrons in the initial state. Consequently, during the rising edges of the laser pulses the electron repulsion has a greater impact on the ionization of the two-electron system, which accounts for our finding that in Li^+ and more clearly in Be^{2+} the electronic interaction notably enhances ionization in contrast to the helium atom.

To elaborate on the impact of the different electronic coupling strengths on the ionization probabilities we have performed calculations for each two-electron system where the laser frequency ω slightly exceeds the binding energy of the respective inner electron. That is, with $\omega=2.25$ a.u. for helium, $\omega=5$ a.u. for Li^+ and $\omega=9$ a.u. for the beryllium ion we have ensured similar conditions for the ionization in each system, where absorption of two photons allows for double ionization. Depicted in Fig. 10 are the ratios of double to single ionization of the three two-electron systems as a function of peak field strength E_0 which has been divided by the cube of the ionic charge Z. This quantity is proportional to the inverse Keldysh parameter γ, therefore being independent of the respective atomic and ionic scales. The ratio between double and single ionization as well as between the according ionization cross sections may be employed to sensitively probe the electron interaction in one-photon break-up processes [61]. However, since exchange and correlation terms are not included in our model, we would rather take it as a measure to discriminate binding effects between the atomic and ionic systems considered here. We have calculated the ratio from the respective ionization probabilities P_1 and P_2 of the inner and outer electron after interaction with a laser pulse of 12 cycles total duration via

$$P_{\text{double}}/P_{\text{single}} = \frac{P_1 P_2}{P_1(1-P_2)+P_2(1-P_1)}. \tag{13}$$

As can be seen in Fig. 10, this quantity shows different behavior in all three systems considered here. According to Eq. (13) the absolute values of the ratio decreases with in-

creasing charge state Z, which is in compliance with the overall decrease of the respective ionization probabilities P_1 and P_2 of the inner and outer electron in the high-frequency regime. This decrease of both the P_i with the nuclear charge Z is in contrast to the results of classical Monte Carlo calculations [58], where the ionization probabilities of hydrogenlike ions have been found to show similar behavior when the laser field frequencies and peak strengths are scaled with Z^2 and Z^3, respectively. This difference is due to the fact that the results of our two-dimensional model calculation show a somewhat different scaling behavior with respect to E_0 and ω compared to the three-dimensional Coulomb potential, therefore the absolute values of the ionization probabilities are not invariant with respect to an increase in Z. To circumvent this deficiency, we expect the role of the interaction between the two electrons to be revealed rather by contrasting the slopes of the ratios between double and single ionization. After a steep increase with field strength E_0 they exhibit a broad maximum, followed by a reduction to about a third its peak value. For both the ions Li^+ and Be^{2+} again an increase of this ratio for $E_0/Z^3 > 2.5$ can be observed, which in He is only present at the highest peak field strengths considered here. For the latter, an additional increase at about $E_0/Z^3 = 2.3$ is present, which is a signature of the ionization suppression effect of the outer electron which has been discussed in Sec. IV C. Comparison between the three systems shows that the width of the maximum at $E_0/Z^3 \approx 0.75$ slightly broadens with increasing charge Z, while its position is shifted to higher peak field strengths. This shows that in the case of ions double ionization rises more rapidly than in helium, such that the electronic interaction becomes more significant with larger nuclear charge. We conclude that these differences in the ratios displayed in Fig. 10 arise due to the different coupling strengths of outer and inner electron in the two-electron systems considered here. This is most apparent for higher field strengths ($E_0/Z^3 > 2.5$), where the increase in the ratios becomes steeper with Z. This is in line with Fig. 7 and Fig. 8, where the electronic interaction was shown to have a greater impact on heliumlike ions with rising nuclear charge. Therefore, with increasing nuclear charge single ionization is progressively suppressed in favor of double ionization. As an explanation, we believe this to arise from the fact that the electrons are bound closer to the nucleus for higher charge such that repulsion plays a larger role.

V. CONCLUSIONS

In this paper, we have numerically investigated the stabilization of two-electron atoms and ions in intense laser pulses beyond the dipole approximation. Employing a two-dimensional model atom, we were able to include the retardation of the laser pulse in our calculations. The Lorentz force does not only lead to a displacement of the electrons in the laser propagation direction, it also promotes the ionization of the electrons, most notably for laser intensities where the stabilization effect breaks down again. Despite this effect, it has been shown that stabilization occurs for helium as well as for Li^+ and Be^{2+}. The repulsive interaction between both electrons leads to strong modifications of the ionization dynamics, but does not destroy the stabilization effect. Employing trapezoidal laser pulses in our calculations, we were able to separate pulse-length dependent effects in the stabilization of helium. Depending on the specific number of optical cycles at each stage of the laser pulse, we observe the existence of a regime of ionization suppression of the outer electron.

ACKNOWLEDGMENTS

The authors acknowledge partial funding of this work from the German Research Foundation (Nachwuchsgruppe within Sonderforschungsbereich 276) and from DFG Grant No. KE 721/1-1.

[1] G. A. Mourou, C. P. J. Barty, and M. D. Perry, Phys. Today **51**, 22 (1998); M. D. Perry *et al.*, Opt. Lett. **24**, 160 (1999); T. Tajima and G. Mourou, Phys. Rev. ST Accel. Beams **5**, 031301 (2002).

[2] *TESLA Technical Design Report*, edited by G. Materlik and T. Tschentscher (DESY, Hamburg, 2001); V. Ayvazyan *et al.*, Phys. Rev. Lett. **88**, 104802 (2003).

[3] M. Gavrila, *Atoms in Intense Laser Fields* (Academic, New York, 1992); M. Protopapas, C. H. Keitel, and P. L. Knight, Rep. Prog. Phys. **60**, 389 (1997); C. J. Joachain, M. Dörr, and N. Kylstra, Adv. At., Mol., Opt. Phys. **42**, 225 (2000); C. H. Keitel, Contemp. Phys. **42**, 353 (2001); A. Maquet and R. Grobe, J. Mod. Opt. **49**, 2001 (2002).

[4] D. B. Miloševic and F. Ehlotzky, Adv. At., Mol., Opt. Phys. **49**, 373 (2003).

[5] Y. I. Salamin, S. X. Hu, K. Z. Hatsagortsyan, and C. H. Keitel, Phys. Rep. **427**, 41 (2006).

[6] A. l'Huillier, L. A. Lompre, G. Mainfray, and C. Manus, Phys. Rev. A **27**, 2503 (1983); S. Augst, D. D. Meyerhofer, D. Strickland, and S. L. Chin, J. Opt. Soc. Am. B **8**, 858 (1991); D. N. Fittinghoff, P. R. Bolton, B. Chang, and K. C. Kulander, Phys. Rev. Lett. **69**, 2642 (1992); K. Yamakawa, Y. Akahane, Y. Fukuda, M. Aoyama, N. Inoue, H. Ueda, and T. Utsumi, *ibid.* **92**, 123001 (2004).

[7] B. Walker, B. Sheehy, L. F. Di Mauro, P. Agostini, K. J. Schafer, and K. C. Kulander, Phys. Rev. Lett. **73**, 1227 (1994); B. Sheehy, R. Lafon, M. Widmer, B. Walker, L. F. Di Mauro, P. A. Agostini, and K. C. Kulander, Phys. Rev. A **58**, 3942 (1998).

[8] A. D. Bandrauk, *Molecules in Laser Fields* (Dekker, New York, 1993); A. Talebpour, S. Larochelle, and S. L. Chin, J. Phys. B **30**, L245 (1997); C. Cornaggia and P. Hering, *ibid.* **31**, L503 (1998); S. M. Hankin, D. M. Villeneuve, P. B. Corkum, and D. M. Rayner, Phys. Rev. Lett. **84**, 5082 (2000); F. Grasbon, G. G. Paulus, S. L. Chin, H. Walther, J. Muth-Bohm, A. Becker, and F. H. M. Faisal, Phys. Rev. A **63**, 041402(R)

(2001).
[9] A. McPherson, B. D. Thompson, A. B. Borisov, K. Boyer, and C. K. Rhodes, Nature (London) **370**, 631 (1994); E. E. B. Campbell, K. Hansen, K. Hoffmann, G. Korn, M. Tchaplyguine, M. Wittmann, and I. V. Hertel, Phys. Rev. Lett. **84**, 2128 (2000); H. Wabnitz *et al.*, Nature (London) **420**, 482 (2002); E. Cormier, P.-A. Hervieux, R. Wiehle, B. Witzel, and H. Helm, Eur. Phys. J. D **26**, 83 (2003).
[10] H. D. Jones and H. R. Reiss, Phys. Rev. B **16**, 2466 (1977); Gy. Farkas, Cs. Tóth, S. D. Moustaizis, N. A. Papadogiannis, and C. Fotakis, Phys. Rev. A **46**, R3605 (1992); P. A. Norreys *et al.*, Phys. Rev. Lett. **76**, 1832 (1996); K. Z. Hatsagortsyan and C. H. Keitel, J. Phys. B **35**, L175 (2002).
[11] L. F. DiMauro and P. Agostini, Adv. At., Mol., Opt. Phys. **35**, 79 (1995); R. Dörner *et al.*, *ibid.* **48**, 1 (2002).
[12] T. Weber *et al.*, Phys. Rev. Lett. **84**, 443 (2000); R. Moshammer *et al.*, *ibid.* **84**, 447 (2000).
[13] V. L. B. de Jesus *et al.*, J. Phys. B **37**, L161 (2004).
[14] E. Eremina *et al.*, Phys. Rev. Lett. **92**, 173001 (2004).
[15] A. Becker and F. H. M. Faisal, J. Phys. B **29**, L197 (1996); Phys. Rev. A **59**, R1742 (1999); S. P. Goreslavskii, S. V. Popruzhenko, R. Kopold, and W. Becker, *ibid.* **64**, 053402 (2001); C. Figueira de Morisson Faria, H. Schomerus, X. Liu, and W. Becker, *ibid.* **69**, 043405 (2004); A. Becker and F. H. M. Faisal, J. Phys. B **38**, R1 (2005).
[16] C. A. Ullrich and E. K. U. Gross, Comments At. Mol. Phys. **33**, 211 (1997); M. Petersilka and E. K. U. Gross, Laser Phys. **9**, 105 (1999); D. Bauer and F. Ceccherini, Opt. Express **8**, 377 (2001).
[17] P. J. Ho, R. Panfili, S. L. Haan, and J. H. Eberly, Phys. Rev. Lett. **94**, 093002 (2005).
[18] H. W. van der Hart and K. Burnett, Phys. Rev. A **62**, 013407 (2000); G. L. Yudin and M. Y. Ivanov, *ibid.* **63**, 033404 (2001).
[19] P. G. Burke, P. Francken, and C. J. Joachain, Europhys. Lett. **13**, 670 (1990); J. Phys. B **24**, 761 (1991); J. Purvis, M. Dorr, M. Terao-Dunseath, C. J. Joachain, P. G. Burke, and C. J. Noble, Phys. Rev. Lett. **71**, 3943 (1993).
[20] R. Grobe and J. H. Eberly, Phys. Rev. A **47**, R1605 (1993); O. V. Ovodova, A. M. Popov, and O. V. Tikhonova, Zh. Eksp. Teor. Fiz. **112**, 470 (1997) [JETP **85**, 257 (1997)]; D. G. Lappas and R. van Leeuwen, J. Phys. B **31**, L249 (1998); M. Lein, E. K. U. Gross, and V. Engel, Phys. Rev. Lett. **85**, 4707 (2000).
[21] R. Grobe and J. H. Eberly, Phys. Rev. A **48**, 4664 (1993).
[22] D. Bauer, Phys. Rev. A **56**, 3028 (1997); D. Bauer and F. Ceccherini, *ibid.* **60**, 2301 (1999).
[23] C. Ruiz, L. Plaja, J. R. Vázquez de Aldana, and L. Roso, Phys. Rev. A **68**, 023409 (2003); Appl. Phys. B: Lasers Opt. **78**, 829 (2004).
[24] J. Prager and C. H. Keitel, J. Phys. B **35**, L167 (2002).
[25] A. Staudt, J. Prager, and C. H. Keitel, Europhys. Lett. **62**, 691 (2003).
[26] S. X. Hu and L. A. Collins, Phys. Rev. A **69**, 033405 (2004).
[27] J. Parker, K. T. Taylor, C. W. Clark, and S. Blodgett-Ford, J. Phys. B **29**, L33 (1996); J. S. Parker, L. R. Moore, K. J. Meharg, D. Dundas, and K. T. Taylor, *ibid.* **34**, L69 (2001); J. S. Parker, B. J. S. Doherty, K. J. Meharg, and K. T. Taylor, *ibid.* **36**, L393 (2003).
[28] M. Dammasch, M. Dörr, U. Eichmann, E. Lenz, and W. Sandner, Phys. Rev. A **64**, 061402(R) (2001); E. A. Chowdhury and B. C. Walker, J. Opt. Soc. Am. B **20**, 109 (2003); E. Gubbini, U. Eichmann, M. Kalashnikov, and W. Sandner, J. Phys. B **38**, L87 (2005).
[29] K. J. Meharg, J. S. Parker, and K. T. Taylor, J. Phys. B **38**, 237 (2005).
[30] J. H. Eberly and K. C. Kulander, Science **262**, 1229 (1993); K. Burnett, V. C. Reed, and P. L. Knight, J. Phys. B **26**, 561 (1993); N. B. Delone and V. P. Krainov, Usp. Fiz. Nauk **165**, 1295 (1995) [Phys. Usp. **38**, 1247 (1995)]; M. V. Fedorov, *ibid.* **169**, 66 (1999) [*ibid.* **42**, 61 (1999)]; M. Gavrila, J. Phys. B **35**, R147 (2002); A. M. Popov, O. V. Tikhonova, and E. A. Volkova, J. Phys. B **36**, R125 (2003).
[31] M. P. de Boer, L. D. Noordam, and H. G. Muller, Phys. Rev. A **47**, R45 (1993).
[32] M. P. de Boer, J. H. Hoogenraad, R. B. Vrijen, L. D. Noordam, and H. G. Muller, Phys. Rev. Lett. **71**, 3263 (1993); M. P. de Boer, J. H. Hoogenraad, R. B. Vrijen, R. C. Constantinescu, L. D. Noordam, and H. G. Muller, Phys. Rev. A **50**, 4085 (1994); N. J. van Druten *et al.*, *ibid.* **55**, 622 (1997).
[33] F. Bloch and A. Nordsieck, Phys. Rev. **52**, 54 (1937); W. Pauli and M. Fierz, Nuovo Cimento **15**, 167 (1938).
[34] H. A. Kramers, *Collected Scientific Papers* (North Holland, Amsterdam, 1956); W. C. Henneberger, Phys. Rev. Lett. **21**, 838 (1968).
[35] M. Gavrila and J. Z. Kamiński, Phys. Rev. Lett. **52**, 613 (1984); M. Pont, N. R. Walet, M. Gavrila, and C. W. McCurdy, *ibid.* **61**, 939 (1988); M. Pont and M. Gavrila, *ibid.* **65**, 2362 (1990).
[36] E. A. Volkova, A. M. Popov, O. V. Smirnova, and O. V. Tikhonova, Zh. Eksp. Teor. Fiz. **111**, 1194 (1997) [JETP **84**, 658 (1997)]; A. M. Popov, O. V. Smirnova, and E. A. Volkova, J. Phys. B **32**, 3331 (1999).
[37] M. H. Mittleman, Phys. Rev. A **42**, 5645 (1990); M. Gavrila and J. Shertzer, *ibid.* **53**, 3431 (1996).
[38] A. Staudt and C. H. Keitel, J. Phys. B **36**, L203 (2003).
[39] J. R. Vázquez de Aldana and L. Roso, Phys. Rev. A **61**, 043403 (2000).
[40] N. J. Kylstra, R. A. Worthington, A. Patel, P. L. Knight, J. R. Vázquez de Aldana, and L. Roso, Phys. Rev. Lett. **85**, 1835 (2000); J. R. Vázquez de Aldana, N. J. Kylstra, L. Roso, P. L. Knight, A. Patel, and R. A. Worthington, Phys. Rev. A **64**, 013411 (2001).
[41] M. W. Walser and C. H. Keitel, J. Phys. B **33**, L221 (2000).
[42] S. Geltman, J. Phys. B **32**, 853 (1999).
[43] K. C. Kulander, Phys. Rev. A **36**, 2726 (1987).
[44] J. B. Watson, A. Sanpera, D. G. Lappas, P. L. Knight, and K. Burnett, Phys. Rev. Lett. **78**, 1884 (1997); K. Burnett, J. B. Watson, A. Sanpera, and P. L. Knight, Philos. Trans. R. Soc. London, Ser. A **356**, 317 (1998); A. Sanpera *et al.*, J. Phys. B **31**, L841 (1998).
[45] S. X. Hu and C. H. Keitel, Phys. Rev. A **63**, 053402 (2001).
[46] J. Javanainen, J. H. Eberly, and Q. Su, Phys. Rev. A **38**, 3430 (1988).
[47] J. Fleck, J. Morris, and M. Feit, Appl. Phys. **10**, 129 (1976); R. W. Heather, Comput. Phys. Commun. **63**, 446 (1991).
[48] S. X. Hu and C. H. Keitel, Europhys. Lett. **47**, 318 (1999).
[49] A. D. Bandrauk and H. Shen, Chem. Phys. Lett. **176**, 428 (1991); J. Chem. Phys. **99**, 1185 (1993).
[50] E. S. Smyth, J. S. Parker, and K. T. Taylor, Comput. Phys.

Commun. **114**, 1 (1998); R. Grobe, S. L. Haan, and J. H. Eberly, *ibid.* **117**, 200 (1999).
[51] C. Szymanowski, R. Panfili, W.-C. Liu, S. L. Haan, and J. H. Eberly, Phys. Rev. A **61**, 055401 (2000).
[52] W. H. Press, S. A. Teukolsky, W. T. Vetterling, and B. P. Flannery, *Numerical Recipes in C* (Cambridge University Press, Cambridge, 1992).
[53] P. Lambropoulos, Phys. Rev. Lett. **55**, 2141 (1985).
[54] T. Katsouleas and W. B. Mori, Phys. Rev. Lett. **70**, 1561 (1993); A. Bugacov, M. Pont, and R. Shakeshaft, Phys. Rev. A **48**, R4027 (1993).
[55] K. C. Kulander, K. J. Schafer, and J. L. Krause, Phys. Rev. Lett. **66**, 2601 (1991); V. C. Reed, P. L. Knight, and K. Burnett, *ibid.* **67**, 1415 (1991).
[56] M. Dondera, H. G. Muller, and M. Gavrila, Phys. Rev. A **65**, 031405(R) (2002); M. Boca, H. Muller, and M. Gavrila, J. Phys. B **37**, 147 (2004).
[57] A. Staudt, C. H. Keitel, and J. S. Briggs, J. Phys. B **39**, 633 (2006).
[58] L. N. Gaier and C. H. Keitel, Phys. Rev. A **65**, 023406 (2002).
[59] R. C. Forrey, H. R. Sadeghpour, J. D. Baker, J. D. Morgan III, and A. Dalgarno, Phys. Rev. A **51**, 2112 (1995); H. W. van der Hart and L. Feng, J. Phys. B **34**, L601 (2001).
[60] A. Patel, N. J. Kylstra, and P. L. Knight, Opt. Express **4**, 496 (1999); J. Phys. B **32**, 5759 (1999).
[61] F. W. Byron, Jr. and C. J. Joachain, Phys. Rev. **164**, 1 (1967); R. Dörner *et al.*, Phys. Rev. Lett. **76**, 2654 (1996); J. A. R. Samson, W. C. Stolte, Z. X. He, J. N. Cutler, Y. Lu, and R. J. Bartlett, Phys. Rev. A **57**, 1906 (1998).